Supporting Information

Simultaneously Enhancing Catalytic Performance and Increasing Density of Bifunctional CuN_3 Active Sites in Dopant-Free 2D C_3N_3Cu for Oxygen Reduction/Evolution Reactions

Jinzhi Tang[⊥a], Zhihao Zeng[⊥a], Haikuan Liang[a], Zhihao Wang[a], Wei Nong[a], Zhen Yang[*b], Chenze Qi[b], Zhengping Qiao[a], Yan Li[*a] and Chengxin Wang[a]

[a]State Key Laboratory of Optoelectronic Materials and Technologies, School of Materials Science and Engineering, Sun Yat-sen (Zhongshan) University, Guangzhou 510275, People's Republic of China

[b]Zhejiang Key Laboratory of Alternative Technologies for Fine Chemicals Process, College of Chemistry and Chemical Engineering, Shaoxing University, Shaoxing, People's Republic of China

* Corresponding authors. E-mail: yangzhen09@usx.edu.cn (Zhen Yang)
liyan266@mail.sysu.edu.cn (Yan Li)

⊥ These authors contributed equally.

Content

S-1 Computational details

In this study, we explored ORR and OER proceeding via four electrons ($4e^-$) pathway as described by Eq 1a-1d and Eq 2a-2d.

The 4e ORR process is as follows:[1-2]

$$O_2\,(g) + H_2O + e^- + * \rightarrow *OOH + OH^- \quad \textbf{(1a)}$$

$$*OOH + e^- \rightarrow *O + OH^- \quad \textbf{(1b)}$$

$$*O + H_2O + e^- \rightarrow *OH + OH^- \quad \textbf{(1c)}$$

$$*OH + e^- \rightarrow OH^- + * \quad \textbf{(1d)}$$

where * indicates an active site of the catalyst, (g) represent the gas phase.

The OER is the reverse reaction of ORR.[3-4]

$$OH^- + * \rightarrow *OH + e^- \quad \textbf{(2a)}$$

$$*OH + OH^- \rightarrow *O + H_2O + e^- \quad \textbf{(2b)}$$

$$*O + OH^- \rightarrow *OOH + e^- \quad \textbf{(2c)}$$

$$*OOH + OH^- \rightarrow O_2\,(g) + H_2O + e^- + * \quad \textbf{(2d)}$$

The cohesive energy (E_c) is defined as

$$E_c = (E_t - \Sigma_i\, n_i E_i)/n \quad \textbf{(3)}$$

where E_t is the total energy of systems, n_i and E_i are the number of the isolated i atom (i = C, N, Cu, Ni and Zn) in unit cell and the corresponding energies, respectively, and $n = \Sigma_i n_i$ is the total number of atoms.

The adsorption energy of adsorbed molecules on the substrate is calculated by

$$E_{ad} = E_{mol+sub} - E_{mol} - E_{sub} \quad \textbf{(4)}$$

where $E_{mol+sub}$, E_{mol}, E_{sub} and are the total energy of adsorption system, adsorbates, and, substrate respectively.

The free energy change for each step can be calculated based on the computational hydrogen electrode (CHE) model of Nøskov et al. by the following equation:[5-6]

$$\Delta G = \Delta E - T\Delta S + \Delta ZPE \quad \textbf{(5)}$$

where ΔE is the energy discrepancy between initial state and final state in reaction.

ZPE is zero-point energy and *S* is the entropy. The entropy and vibration frequency of the molecules in the gas phase are referred from the NIST database. The vibration frequency of adsorbed species can be obtained by calculating with fixed substrate. The direct calculation of the free energy of an oxygen molecule is usually avoided because its ground state is a triplet state. Instead, its free energy is directly derived by this equation:[4]

$$G_{O_2}(\mathrm{g}) = G_{H_2O}(\mathrm{l}) - G_{H_2}(\mathrm{g}) + 4.92\ \mathrm{eV}. \quad \textbf{(6)}$$

G_{H_2O} (l) can be obtained by having the calculation of G_{H_2O} (g) at a pressure of 0.035 bar. And that of $H^+ + e^-$ in solution under standard condition without electrode potential is equal to that of $1/2H_2$ according to the CHE model.[1]

The results of Eq. 1a-1d (ΔG_1, ΔG_2, ΔG_3, ΔG_4) can be calculated separately based on the following equations:

$$\Delta G_1 = \Delta G_{*\mathrm{OOH}} - 4.92 \quad \textbf{(7a)}$$

$$\Delta G_2 = \Delta G_{*\mathrm{O}} - \Delta G_{*\mathrm{OOH}} \quad \textbf{(7b)}$$

$$\Delta G_3 = \Delta G_{*\mathrm{OH}} - \Delta G_{*\mathrm{O}} \quad \textbf{(7c)}$$

$$\Delta G_4 = -\Delta G_{*\mathrm{OH}} \quad \textbf{(7d)}$$

Then, we can derive onset potential (U^{ORR}) and overpotential (η^{ORR}) for ORR from the following equations:

$$U^{\mathrm{ORR}} = -\max(\Delta G_1, \Delta G_2, \Delta G_3, \Delta G_4) \quad \textbf{(8)}$$

$$\eta^{\mathrm{ORR}} = 1.23 - U^{\mathrm{ORR}} \quad \textbf{(9)}$$

The results of Eq. 2a-2d (ΔG_5, ΔG_6, ΔG_7, ΔG_8) is the opposite of Eq. 1a-1d (ΔG_1, ΔG_2, ΔG_3, ΔG_4).

$$\Delta G_5 = \Delta G_{*\mathrm{OH}} \quad \textbf{(10a)}$$

$$\Delta G_6 = \Delta G_{*\mathrm{O}} - \Delta G_{*\mathrm{OH}} \quad \textbf{(10b)}$$

$$\Delta G_7 = \Delta G_{*\mathrm{OOH}} - \Delta G_{*\mathrm{O}} \quad \textbf{(10c)}$$

$$\Delta G_8 = 4.92 - \Delta G_{\mathrm{OOH}*} \quad \textbf{(10d)}$$

Similarly, the calculation of U^{OER} and η^{OER} can be expressed as follows:

$$U^{\mathrm{OER}} = \max(\Delta G_5, \Delta G_6, \Delta G_7, \Delta G_8) \quad \textbf{(11)}$$

$$\eta^{\mathrm{OER}} = U^{\mathrm{OER}} - 1.23 \quad \textbf{(12)}$$

The average energy of *d* band near the Fermi energy for transition metal atoms is calculated by[7]

$$d_{center} = \frac{\int_{-0.5}^{0}(\varepsilon \times \rho)d\varepsilon}{\int_{-0.5}^{0}\rho d\varepsilon} \quad \textbf{(13)}$$

where ρ the electron density at certain energy level of ε.

S-2 Structural Details

1. Coordinate information of C_3N_3Cu in .cif file

data_CONTCAR-C_3N_3Cu
_audit_creation_date 2022-04-04
_audit_creation_method 'Materials Studio'
_symmetry_space_group_name_H-M 'P-3'
_symmetry_Int_Tables_number 147
_symmetry_cell_setting trigonal
loop_
_symmetry_equiv_pos_as_xyz
x,y,z
-y,x-y,z
-x+y,-x,z
-x,-y,-z
y,-x+y,-z
x-y,x,-z
_cell_length_a 6.5319
_cell_length_b 6.5319
_cell_length_c 21.2860
_cell_angle_alpha 90.0000
_cell_angle_beta 90.0000
_cell_angle_gamma 120.0000
loop_
_atom_site_label
_atom_site_type_symbol
_atom_site_fract_x
_atom_site_fract_y
_atom_site_fract_z
_atom_site_U_iso_or_equiv
_atom_site_adp_type
_atom_site_occupancy
N1 N 0.54628 0.94722 0.01711 0.01267 Uiso 1.00
C1 C 0.76890 0.97819 0.00221 0.01267 Uiso 1.00
Cu1 Cu 0.33333 0.66667 0.05797 0.01267 Uiso 1.00

2. Coordinate information of C_3N_3Ni in .cif file

```
data_CONTCAR-C3N3Ni
_audit_creation_date              2022-04-04
_audit_creation_method            'Materials Studio'
_symmetry_space_group_name_H-M    'P-3'
_symmetry_Int_Tables_number       147
_symmetry_cell_setting            trigonal
loop_
_symmetry_equiv_pos_as_xyz
  x,y,z
  -y,x-y,z
  -x+y,-x,z
  -x,-y,-z
  y,-x+y,-z
  x-y,x,-z
_cell_length_a                    6.5116
_cell_length_b                    6.5116
_cell_length_c                    21.2601
_cell_angle_alpha                 90.0000
_cell_angle_beta                  90.0000
_cell_angle_gamma                 120.0000
loop_
_atom_site_label
_atom_site_type_symbol
_atom_site_fract_x
_atom_site_fract_y
_atom_site_fract_z
_atom_site_U_iso_or_equiv
_atom_site_adp_type
_atom_site_occupancy
N1     N     0.54380   0.94234   0.01638   0.01267  Uiso   1.00
C1     C     0.76771   0.97517   0.00224   0.01267  Uiso   1.00
Ni1    Ni    0.33333   0.66667   0.05595   0.01267  Uiso   1.00
```

3. Coordinate information of C_3N_3Zn in .cif file

```
data_CONTCAR-C3N3Zn
_audit_creation_date              2022-04-04
_audit_creation_method            'Materials Studio'
_symmetry_space_group_name_H-M    'P-3'
_symmetry_Int_Tables_number       147
_symmetry_cell_setting            trigonal
loop_
```

```
_symmetry_equiv_pos_as_xyz
  x,y,z
  -y,x-y,z
  -x+y,-x,z
  -x,-y,-z
  y,-x+y,-z
  x-y,x,-z
_cell_length_a                 6.4668
_cell_length_b                 6.4668
_cell_length_c                 21.5395
_cell_angle_alpha               90.0000
_cell_angle_beta                90.0000
_cell_angle_gamma                 120.0000
loop_
_atom_site_label
_atom_site_type_symbol
_atom_site_fract_x
_atom_site_fract_y
_atom_site_fract_z
_atom_site_U_iso_or_equiv
_atom_site_adp_type
_atom_site_occupancy
N1    N    0.53553   0.92861   0.01142   0.01267  Uiso   1.00
C1    C    0.76393   0.97157   0.00126   0.01267  Uiso   1.00
Zn1   Zn   0.33333   0.66667   0.07452   0.01267  Uiso   1.00
```

S-3 For Section 3.1

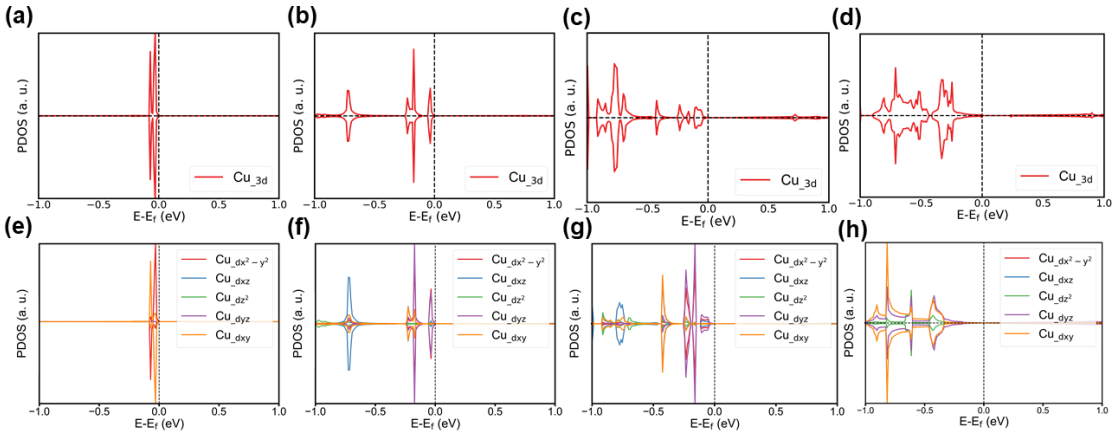

Figure S1. (a-d) The PDOS of Cu_3*d* and (e-h) PDOS onto dx^2-y^2, dxz, dz^2, dyz, and dxy for 1-CuN_3, 2-CuN_3, 3-CuN_3, C_3N_3Cu, respectively.

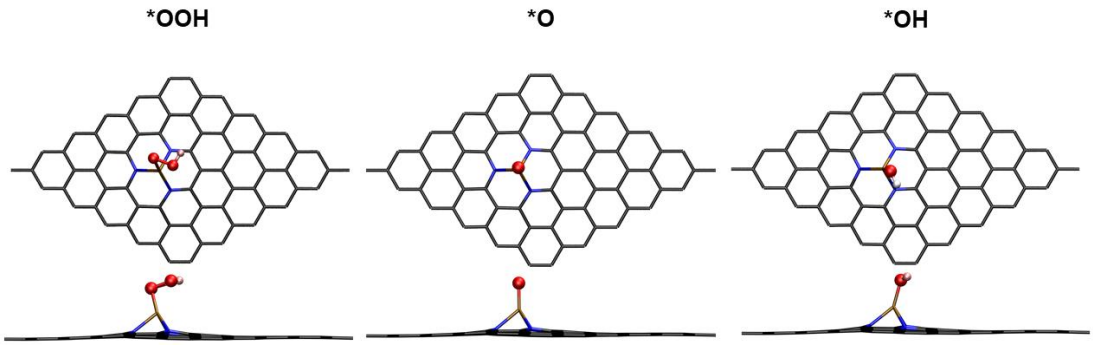

Figure S2. Structural configurations of reaction intermediates of *OOH, *O and *OH on 1-CuN_3.

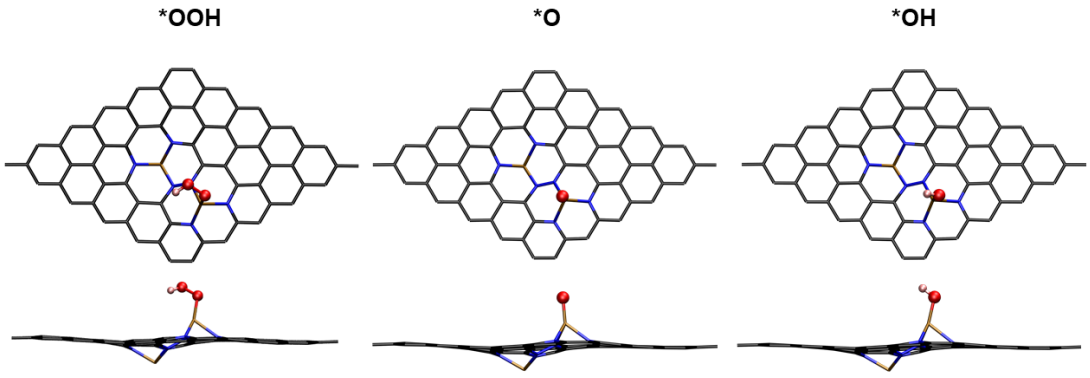

Figure S3. Structural configurations of reaction intermediates of *OOH, *O and *OH on 2-CuN_3.

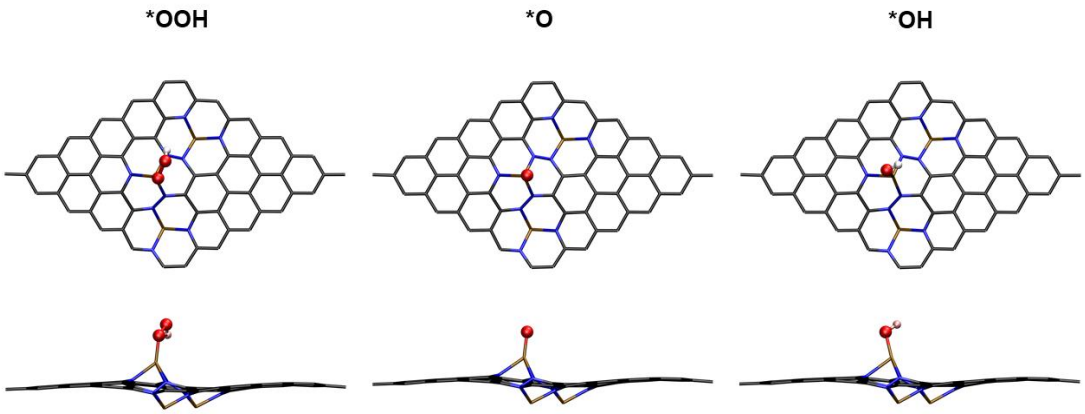

Figure S4. Structural configurations of reaction intermediates of *OOH, *O and *OH on 3-CuN_3.

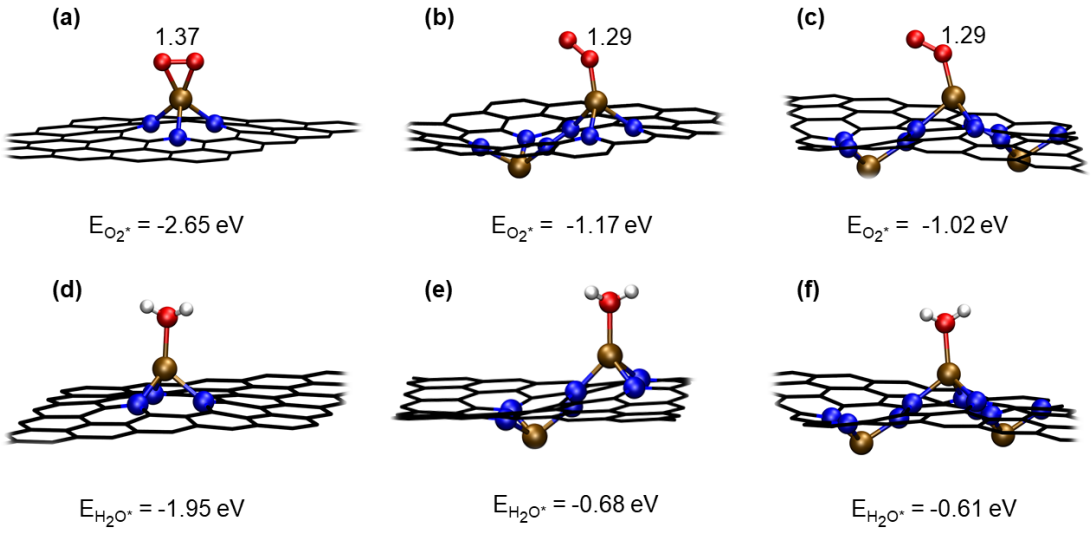

Figure S5. The optimized structural configurations of O_2* and H_2O* on (a, d)1-CuN_3, (b, e) 2-CuN_3 and (c, f) 3-CuN_3. The bond length of O-O of O_2* and adsorption energy of O_2* and H_2O* were illustrated, with the unit of bond length of Å.

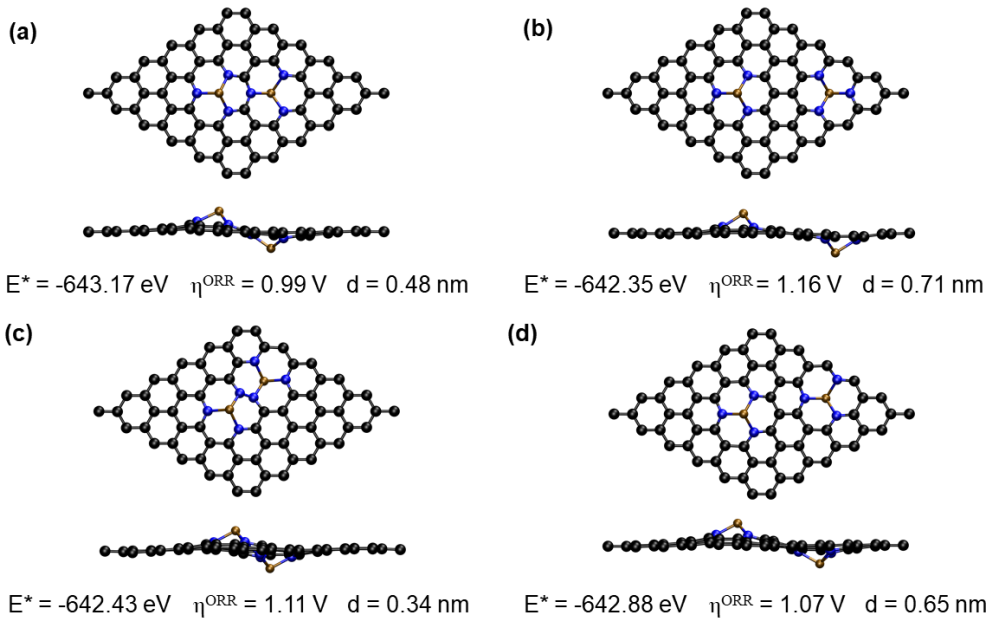

Figure S6. Different structural configurations of 2-CuN_3. Energy of substrate (E*), over potential of ORR (η^{ORR}), horizontal distance between two Cu atoms among them (d) were illustrated. Models (a), (b) and (d) show two CuN_3 sites that are not directly adjacent to each other in graphene, and the distances between them are 0.48, 0.71, and 0.65 nm, respectively. The model (c) with two connected CuN_3 was selected as representative for 2-CuN_3 because this type arrangement of CuN_3 is promising for designing 2D catalysts with high concentration of CuN_3 moiety.

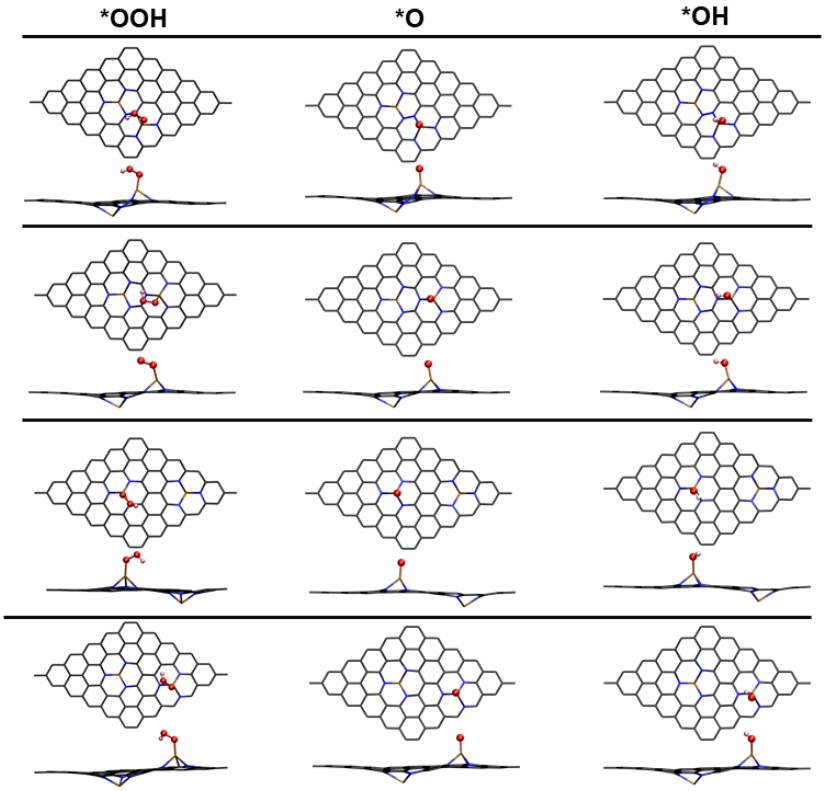

Figure S7. Structural configurations of reaction intermediates of *OOH, *O and *OH on 2-CuN_3 with four possible arrangements of CuN_3 moieties.

S-4 For Section 3.2

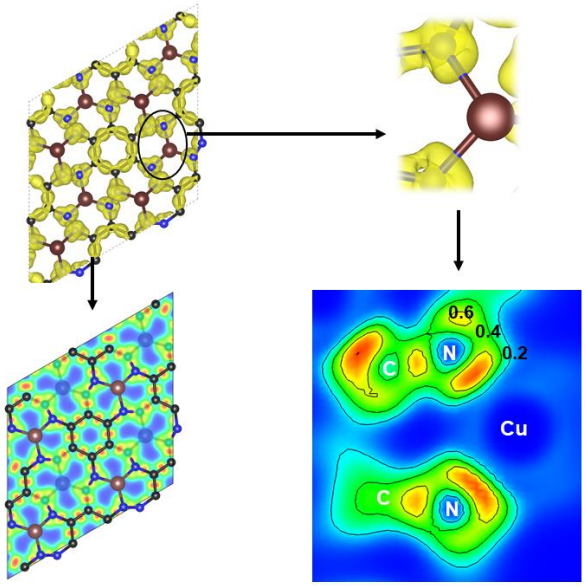

Figure. S8 The electron localization function (ELF) of C_3N_3Cu. The C, N and Cu atoms are marked in white color. The isosurface levels are set at 0.50 e/r_0^3.

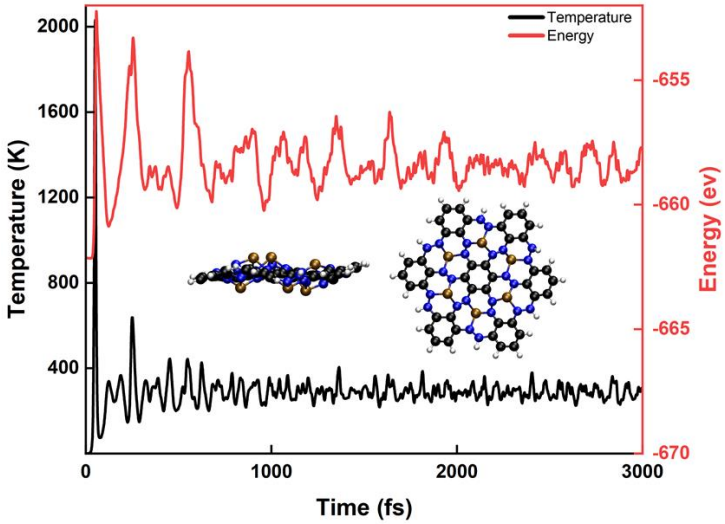

Figure. S9 AIMD simulations of C_3N_3Cu nano flake. The lateral and top views of strcture snapshot at the end of AIMD simulations is illustrated.

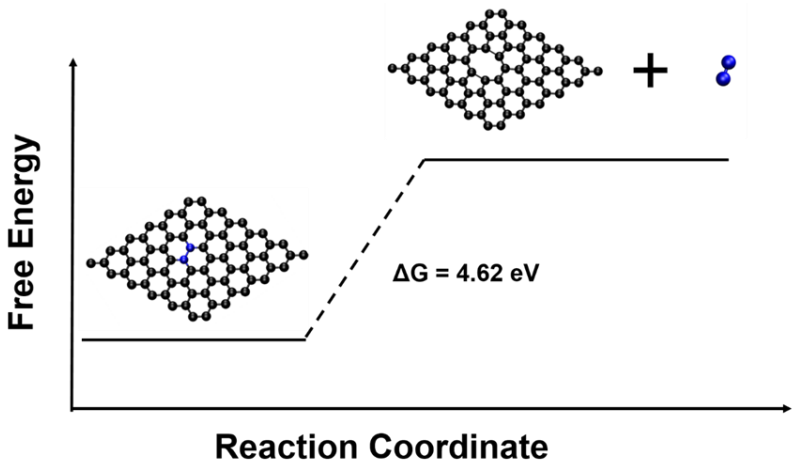

Figure. S10 The free energy diagram of N_2 formation by the decomposition process of the N-N bonds in graphene leaving leading to the formation of two rings of 5 fold and 9 fold in the carbon lattice.

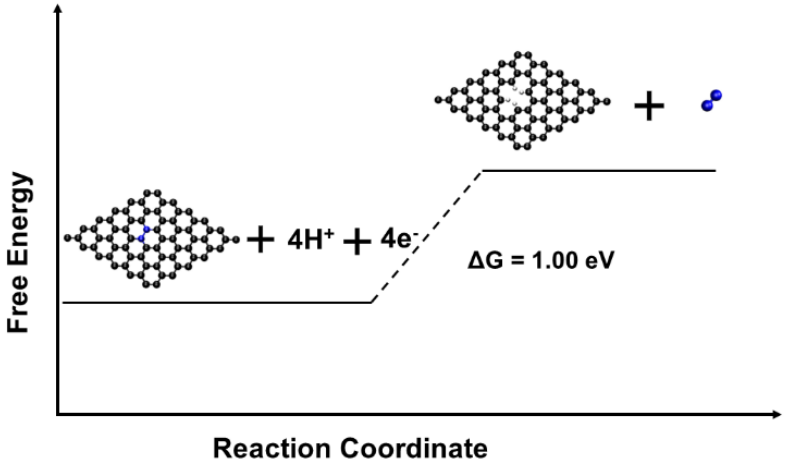

Figure. S11 The free energy diagram of -C-H formation by the decomposition process of the N-N bonds in graphene.

Table S1. The Wyckoff positions and coordinates of N, C and Cu in C_3N_3Cu.

Element	Wyckoff Position	Coordinate
N	6g	(0.54637 0.94740 0.01717)
C	6g	(0.76908 0.97823 0.00222)
Cu	2d	(0.33333 0.66667 0.05806)

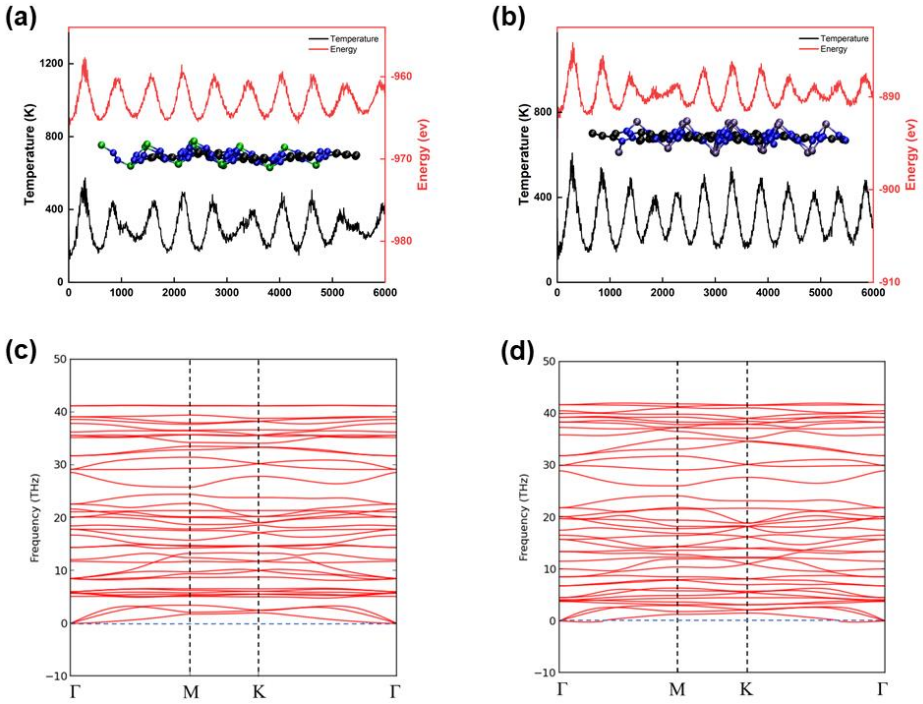

Figure. S8 (a, b) AIMD simulations at 300K of C_3N_3Ni and C_3N_3Zn. (c, d) phonon spectrums of C_3N_3Ni and C_3N_3Zn. The lateral views of monolayers at the end of AIMD simulations are illustrated in the insets (a, b).

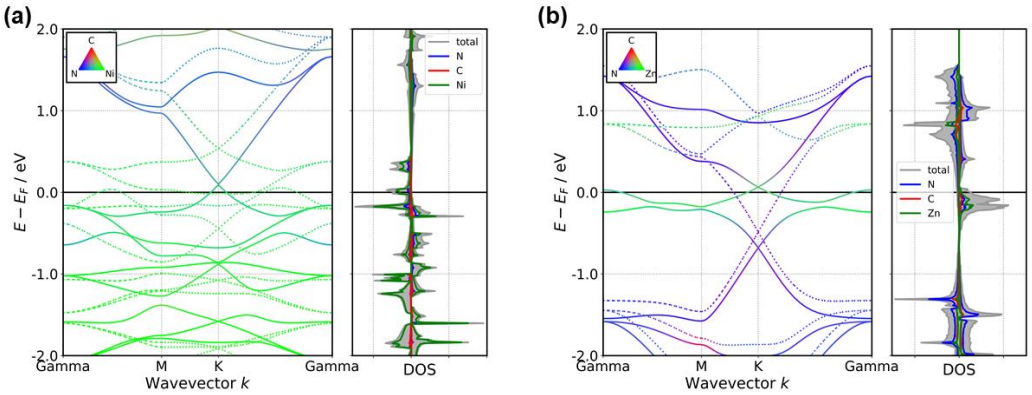

Figure. S9 The elemental projected band and DOS of (a) C_3N_3Ni and (b) C_3N_3Zn. The Fermi level (E_f) is set to zero.

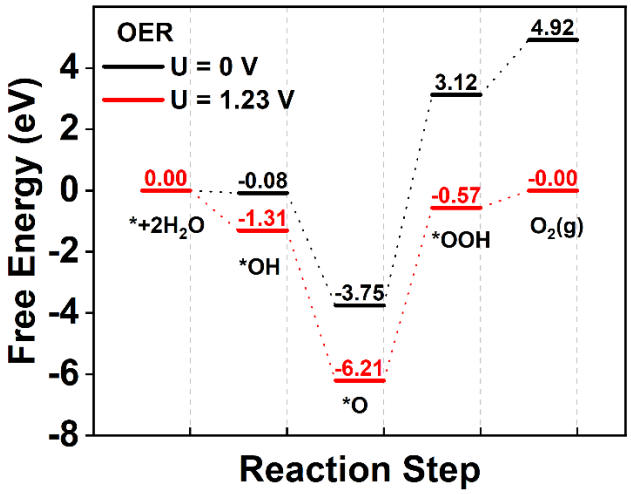

Figure. S10 Free energy profiles of OER over C_3N_3Ni.

Reference

(1) Nørskov, J. K.; Rossmeisl, J.; Logadottir, A.; Lindqvist, L.; Kitchin, J. R.; Bligaard, T.; Jónsson, H. Origin of the Overpotential for Oxygen Reduction at a Fuel-Cell Cathode. *J. Phys. Chem. B* **2004,** *108* (46), 17886-17892.

(2) Stamenkovic, V.; Mun, B. S.; Mayrhofer, K. J. J.; Ross, P. N.; Markovic, N. M.; Rossmeisl, J.; Greeley, J.; Nørskov, J. K. Changing the Activity of Electrocatalysts for Oxygen Reduction by Tuning the Surface Electronic Structure. *Angew. Chem., Int. Ed.* **2006,** *45* (18), 2897-2901.

(3) Man, I. C.; Su, H.-Y.; Calle-Vallejo, F.; Hansen, H. A.; Martínez, J. I.; Inoglu, N. G.; Kitchin, J.; Jaramillo, T. F.; Nørskov, J. K.; Rossmeisl, J. Universality in Oxygen Evolution Electrocatalysis on Oxide Surfaces. *ChemCatChem* **2011,** *3* (7), 1159-1165.

(4) Valdés, Á.; Qu, Z. W.; Kroes, G. J.; Rossmeisl, J.; Nørskov, J. K. Oxidation and Photo-Oxidation of Water on TiO2 Surface. *J. Phys. Chem. C* **2008,** *112* (26), 9872-9879.

(5) Hansen, H. A.; Rossmeisl, J.; Nørskov, J. K. Surface Pourbaix diagrams and oxygen reduction activity of Pt, Ag and Ni(111) surfaces studied by DFT. *Phys. Chem. Chem. Phys.* **2008,** *10* (25), 3722-3730.

(6) Zhai, L.; Sun, Y.; Yang, J.; Wang, H.; Li, Z.; Xia, M.; Gao, F.; Wang, J. Moderate Adsorption of Oxygen Molecular Induced Better Performance of Oxygen Reduction Reaction. *J. Electrochem. Soc.* **2019,** *166* (6), F386-F392.

(7) Choi, D.; Jung, J. Y.; Lee, M. J.; Kim, S.-h.; Lee, S.; Lee, D. W.; Kim, D.-g.; Kim, N. D.; Lee, K.-S.; Kim, P.; Yoo, S. J. Atomic Rearrangement in Core–Shell Catalysts Induced by Electrochemical Activation for Favorable Oxygen Reduction in Acid Electrolytes. *ACS Catal.* **2021,** *11* (24), 15098-15109.